**RC24757 (W0903-021) March 6, 2009**
**Electrical Engineering**

# IBM Research Report

## The Microstructure and Crystal Orientation of Sn-Ag and Sn-Cu Solders Affected by Their Interfacial Reactions with Cu and Ni(P)

**Sun-Kyoung Seo[1], Sung K. Kang[2], Moon Gi Cho[1], Da-Yuan Shih[2], Hyuck Mo Lee[1,3]**

[1]Department of Materials Science and Engineering
KAIST
335 Gwahangno, Yuseong-gu
Daejeon 305-701
Republic of Korea

[2]IBM Research Division
Thomas J. Watson Research Center
P.O. Box 218
Yorktown Heights, NY 10598

[3]email: hmlee@kaist.ac.kr

**Research Division**
**Almaden - Austin - Beijing - Cambridge - Haifa - India - T. J. Watson - Tokyo - Zurich**

## Abstract

Recently, it has been reported that the crystal orientation and grain size of the β-Sn phase in Sn-rich solders have profound effects on the reliabilities of Pb-free solder joints, such as thermo-mechanical fatigue, electromigration, and among others. Additionally, it is also known that the microstructure of Sn-rich solders is strongly affected by their alloy composition. In this study, the grain size and orientation of the β-Sn phase are investigated in terms of their alloy composition and interfacial reactions with two different under bump metallurgy (UBM), Cu vs. Ni(P). Solder balls (380μm in diameter) of pure Sn, Sn-0.5Cu, Sn-0.5Ag and Sn-1.8Ag (in wt%) were reflowed on Cu and Ni(P) UBM. After reflowed at 250°C for 2min, the microstructure of solder joints is analyzed by cross polarization light microscopy and electron backscatter diffraction (EBSD). For the compositional analysis of solder joints, electron probe micro analyzer (EPMA) was used, and thermodynamic calculations were performed to compare with.



Key words: β-Sn grains, Pb-free solders, interfacial reaction, EBSD

## Introduction

The most promising candidates of Pb-free solders are near-eutectic binary Sn-Ag, Sn-Cu and ternary Sn-Ag-Cu [1-4]. However, in these solders, the thick Cu6Sn5 IMC layer and large Ag3Sn primary phase are often reported to influence the integrity and reliability of solder joints [1-4]. In order to improve the reliability of Pb-free solder joints, recently it is proposed to reduce Ag and Cu contents as well as to add minor alloying elements such as Zn, In, Bi, Co, Ni in Sn-based solders [5-10].

Since most Pb-free solders have a composition of more than 90% in Sn, the physical/chemical/electrical properties of Pb-free solders are predominantly affected by the properties of a β-Sn crystal . The properties of Sn are very anisotropic owing to the unique crystal structure of β-Sn, body-centered tetragonal (bct) (a: 5.83, c: 3.18 Å). The coefficient of thermal expansion (CTE) and Young's modulus of β-Sn along c-axis is about two or three times larger than along a-axis as listed in Table 1[11,12]. And, the diffusivity of solute atoms (e.g., Ag, Cu, Ni) in Sn matrix is very different along a- or c-axis. The diffusivity of Ag along c-axis is about 60 times, 40 times for Cu, and 30000 times for Ni, faster than along a-axis at 150°C[13-16]. These anisotropic properties of β-Sn could seriously affect the integrity and reliability of Sn-rich solder joints [17-21].

M. Lu et al. reported a strong correlation between electromigration degradation mechanisms and Sn-grain orientations [17,18]. The consumption of under bump metallurgy (UBM) layer is accelerated near the grain having [001] of a Sn crystal parallel to the direction of the electronical current, reducing the time to failure

(TTF).This result is consistent with the highly anisotropic diffusion behaviors of Cu and Ni solute atoms in Sn as shown in Table 1. In other literatures, D.W. Henderson et al. and S.K. Kang et al. reported that β-Sn grains in SnAgCu solder joints became smaller by the recrstalization process and hence the recrystallized grain boundaries provided an easy path for crack propagation during thermo-mechanical fatigue tests [19, 20].

To enhance the reliability of Pb-free solder joints, the systematic investigation of Sn crystal orientations in Sn-rich solders is needed. There are some previous studies about the fundamental information of β-Sn grains in Sn-rich solders. L.P. Lehman et al. introduced the Kara's beach-ball structure having 60 degree cyclic twins in Sn-Ag-Cu bulk solders [21]. A.U. Telang et al. investigated the changes of size and orientation of β-Sn grains in pure Sn ingot [22]. In our previous studies, the microstructure and crystal orientation of Sn-Cu and Sn-Ag bulk solders were investigated as functions of alloy composition and cooling rate, and the microstructure changes of Sn-Ag and Sn-Cu bulk solders during high temperature aging were also reported [23, 24]. These previous studies were about bulk solders, not about solder joints. In general, when the Sn-rich solders are reacted to UBMs during reflow, the solder joint composition is expected to changed due to the dissolution of UBM into the solder joint. In addition, Sn grain orientations are going to be influenced by the compositional change as well as by the cooling direction of the solder joint.. Therefore, in this study, the grain size and orientation of the β-Sn phase of Sn-rich solders are investigated after the interfacial reactions with two different UBMs, Cu vs. Ni(P).

## Experimental

Solder balls of pure Sn, Sn-0.5Cu, Sn-0.5Ag, and Sn-1.8Ag (380 μm in diameter) commercially produced were used in this study. These solder balls were reflowed on Cu or Ni(P) UBM at 250°C for 2 minute, and then cooled in air. Their cooling rate was estimated to be about 8°C/sec. Figure 1 shows the heat profile during reflow. The UBM structure used in this study is shown in Fig.2. Two kinds of UBM finishes, Cu line/OSP(2μm) and Cu line/Ni(P)(2μm)/Au(500Å) were employed. The total thickness of PCB is 0.9 mm with the thickness of Cu line, 35μm, and an open pad size, 300 μm in diameter. Total ten solder joints were investigated in each condition. For reference, bulk solder balls were also reflowed in the same reflow condition.

The reflowed solder joints and bulk solder balls were cross-sectioned, fine-polished and examined with an optical microscope under cross-polarized imaging conditions. Optical cross-polarization imaging technique has been demonstrated as a useful tool to evaluate the Sn grain size [21-24]. To obtain the information on grain size and Sn crystal orientation, electron backscatter diffraction (EBSD) technique was employed. For quantitative composition analyses of solders, electron probe micro analyzer (EPMA) analysis was conducted.

For the thermodynamic calculations (for binary or ternary phase diagrams and solubility), the Thermo-Calc software developed at the Royal Institute of Technology, Stockholm, Sweden was used [25]. The reported thermodynamic parameters of binary Sn-Cu[26], Sn-Ni[27], ternary Sn-Ag-Cu[28], Sn-Cu-Ni[29] and Sn-Ag-Ni[30] were used for the calculation in this study.

## Result and Discussion

### Sn grain orientation in solder/Cu joints

Figure 3 shows typical cross-polarized images of reflowed bulk solders and solder joints reflowed on Cu UBM. Different color contrasts show the different orientation of Sn grains [22-24] In reflowed bulk solders, pure Sn (380μm) had one large grain or a few large 60 degree twins. Sn grains observed in Sn-0.5Cu were similar to pure Sn, while very fine 60 degree twins were observed in reflowed bulk Sn-0.5Ag and Sn-1.8Ag. The reaction with Cu UBM changed the grain structure in these Sn-rich solders. In pure Sn/Cu and Sn-0.5Cu/Cu joints, columnar grains were observed in all ten samples as shown in Fig.3. In Sn-1.8Ag/Cu joint, one grain (8 samples) and beach-ball shaped 3 or 4 grains (2 samples) were observed. And, in Sn-0.5Ag/Cu joint, the mixture of columnar grains and large grains (100-150μm) were observed in all 10 samples.

The columnar grains in Sn-0.5Cu/Cu joint were analyzed using EBSD for the crystal orientation of β-Sn. Figure 4 shows the result of EBSD analysis of columnar grains. The image quality map in Fig. 4(b) shows grain boundaries noticeably and the inverse pole figure map in Fig. 4(c) shows Sn grain orientations. Columnar Sn grains are parallel to the cooling direction, from the substrate to solder inside. At the interface between solder and Cu UBM, the initial state of cooling, many small grains having various crystal directions were formed, and then, as solidification progressed into the solder

inside, Sn grains having [110] crystal direction, which is the preferred growth direction of Sn dendrites, grew perpendicular to the interface toward the solder inside [31].

Differently from pure Sn/Cu and Sn-0.5Cu/Cu joints, two types of β-Sn grain orientations, one single grain or beach-ball shaped (three or four) grains were observed in Sn-1.8Ag/Cu joints. The result of EBSD analysis for the typical samples is shown in Fig 5. The one grain observed in microscopy image exhibits a low-angle orientation with [100] (<2°). The minor group of beach-ball shaped grains are 60 degree cyclic twins with [100] rotation axis. Comparing with the reflowed bulk Sn-1.8Ag, the fine twins were not observed in Sn-1.8Ag/Cu joints. The crystal direction of Sn grains parallel to the cooling direction is near [100] or [001].

In Sn-0.5Ag/Cu joint, both the microstructure characteristics of Sn-0.5Cu/Cu and Sn-1.8Ag/Cu joints were observed. Columnar grains observed in Sn-0.5Cu/Cu joints were shown near the UBM interface and large grains (>100μm) observed in Sn-1.8Ag/Cu joints were shown inside the solder. Because the Ag wt% in solder is low, Sn0.5Ag/Cu joint has a different microstructure from Sn-1.8Ag/Cu joint.

The reaction with Cu UBM is expected to considerably change the composition in solders, which in turn could cause the microstructure change. To get the information about the composition in solder, EPMA quantitative composition analyses were conducted in the area, 200 μm in diameter, of each solder joint. Table 2 summarizes the results of EPMA analysis. The Cu composition analyzed in four solder/Cu joints is very similar each other, near 1.3 wt%, regardless of the solder compositions..

Cu compositions measured by EPMA were compared with the Cu solubility value in each solder system, which was calculated thermodynamically. For the solubility calculation, thermodynamic parameters of Sn-Cu binary system were used for pure Sn/Cu and Sn-0.5Cu/Cu joints, and those of Sn-Ag-Cu ternary system for Sn-0.5Ag/Cu and Sn-1.8Ag/Cu joints [27, 28]. Using Thermo-Calc program, the Sn-Cu binary, and ternary phase diagrams of Sn-0.5Ag-Cu and Sn-1.8Ag-Cu were constructed as shown in Fig. 6, from which the Cu solubility at 250°C was calculated for each system.. The calculated values of Cu solubility are in good agreement with the Cu composition in each solder measured by EPMA (Table 2). Based on these results, it can be said that Cu atoms were dissolved from UBM and quickly saturated to its solubility limit during 2 min reflow at 250°C. The calculated Cu solubility in Sn-Ag-Cu system is a little smaller than that in Sn-Cu system. This may be due to the slightly enlarged two-phase stable region of liquid and Cu6Sn5 as Ag wt% increases in Sn-Ag-Cu system.

As shown in Fig. 3, a few large grains in pure Sn and Sn-0.5Cu solders change to many columnar grains after the reaction on Cu UBM, having a preferred Sn orientation of <110>. In addition, the fine twins in Sn-Ag solders change to a few large grains after the reaction with Cu UBM. This significant microstructure change is attributed to to the fast dissolution of Cu atoms from the Cu UBM and the subsequent precipitation of various IMCs, affecting the orientation and microstructure of Sn grains.

## Sn orientation in solder/ Ni(P) joints

To compare the effect of Ni(P) UBM with Cu UBM on the changes of Sn grain orientation, the similar interfacial reactions were repeated with pure Sn, Sn-0.5Cu, Sn-0.5Ag and Sn-1.8Ag. Figure 7 shows typical cross-polarized images of solder joints reflowed on Ni(P) UBM. In pure Sn/Ni(P) joints, beach-ball shaped three grains (5 samples) and one grain (5 samples) were observed. In Sn-0.5Cu/Ni(P) joints, all ten samples have beach-ball shaped grains. In Sn-0.5Ag/Ni(P) joints, one grain (7 samples) and small grains(30-150 μm) (3 samples). In Sn1.8Ag/Ni(P) joints, one grain (9 samples) and the mixture of large beach-ball shaped and fine grains (1 sample) were observed in cross-polarized images. Overall, in pure Sn/Ni(P) and Sn-0.5Cu/Ni(P) joints, beach-ball shaped grains are the majority, while in Sn-0.5Ag/Ni(P) and Sn-1.8Ag/Ni(P) joints, one large grain is the majority. These Sn grain orientations observed on Ni UBM are quite different from Sn grain orientations observed on Cu UBM..

For the information about the crystal orientation of beach-ball shaped grains, EBSD analysis was conducted on Sn-0.5Cu/Ni(P) joints, as shown in Fig.8. The beach-ball shaped grains were cyclic twins of Sn. Different from the cyclic twins observed in pure Sn/Ni(P) joints, the cyclic twins of Sn-0.5Cu/Ni(P) joint were subdivided into several grains. As shown in Fig. 8, it has various rotation angles (23, 45, and 60°) with [100] rotation axis.

In Sn-Ag/Ni(P) joints, most samples have one large grain as shown in Fig. 7 and 9. In Fig. 9, Sn-1.8Ag/Ni(P) joint has near [111] crystal directions, which is the same orientation reported by Weinberg et. Al, the preferred direction of Sn-0.005wt% [32]. Although one large grain was the major grain structure, fine twins were occasionally

observed. In one sample of Sn-1.8Ag/Ni(P), the fine twins were observed near the interface between the UBM and solder. In our previous paper, it was reported that as cooling rate and Ag wt% increase, the 60° twins become finer in Sn-Ag solder balls [23]. Since the cooling rate at the interface is expected to be somewhat faster and Ag content is also somewhat higher than the solder inside, the fine 60° twins could be formed near the interface.

In order to find the composition in solder after reacted with Ni(P) UBM, EPMA quantitative composition analysis was conducted in the area of 200 μm in diameter for each solder joint. Table 3 shows the results of EPMA analysis. Comparing with Table 2, the Ni dissolution into solder is confirmed to be much smaller (7-12 times) than the Cu dissolution. The Ni solubility in solder at 250C was calculated thermodynamically for each solder composition. For the solubility calculation, thermodynamic parameters of Sn-Ni binary system were used for pure Sn/Ni joint, Sn-Cu-Ni ternary system for Sn-0.5Cu/Ni joint, and Sn-Ag-Ni ternary system for Sn-Ag/Ni joints [28, 30, 31]. Using Thermo-Calc program, the corresponding binary or ternary phase diagrams were constructed as shown in Fig. 10, from which, the Ni solubility at 250 °C was calculated. The Ni solubility value in Sn-Ni system is similar to Sn-Ag-Ni system. However, the Ni solubility in Sn-Cu-Ni system is smaller than other systems. Because the difference of atomic number between Cu and Ni is one and their atomic radius are similar to each other, the presence of Cu in solder could reduce Ni dissolution from Ni(P) UBM to the liquid solder. In Fig. 10(b), the formation of the two phase region of liquid and Cu6Sn5 reduces the Ni solubility. Although Ni wt% in pure Sn/Ni(P) joint measured by EPMA is smaller than the Ni solubility in Sn-Ni system, Ni wt% in other joints are similar to

the calculated Ni solubility. Namely, in Sn-Cu-Ni and Sn-Ag-Ni systems, Ni atoms were dissolved quickly to the Ni solubility limit during 2min reflow at 250 °C.

The change of Sn grain orientation during the interfacial reaction with Ni(P) UBM is different from the reaction with Cu UBM. The columnar grains in Sn-Cu /Cu joint was not observed in Sn-Cu/Ni(P) joint. Only large cyclic twins were observed in Sn-Cu/Ni(P) joint. In Sn-0.5Cu, about 1.3 wt% of Cu is dissolved from Cu UBM, while 0.06 wt% Ni is dissolved from Ni(P) UBM after the reflow at 250C, 2 min.. The large compositional change of 1.3 wt% Cu is attributed to the formation of columnar grains, while the small compositional change of 0.06wt% Ni in Sn-Cu/Ni joints is attributed to the formation of large twins. The fine twins in bulk Sn-Ag solders are changed to a few large grains after the reaction with Cu or Ni(P) UBM in most samples. The additional precipitation of Cu6Sn5 and Ni3Sn4 together with Ag3Sn could interrupt the formation of fine twins of the Sn matrix.

## Conclusion

The reactions with Cu and Ni(P) UBM strongly affect the Sn orientation in both Sn-Cu and Sn-Ag solders. During reflow on Cu or Ni(P) UBM, Cu and Ni atoms are dissolved quickly and saturate to their solubility limits in solders, causing the changes in composition and microstructure. A few large grains in pure Sn and Sn-0.5Cu solders change to many columnar grains after the reaction on Cu UBM, with the large compositional change of 1.3wt% Cu, while a few large grains are maintained after the reaction on Ni(P) UBM, with the small compositional change of 0.07wt% Ni. The fine

twins in Sn-Ag solders change to a few large grains after the reaction with Cu or Ni(P) UBM. This microstructure change is attributed to the compositional changes during reflow and subsequent precipitation of IMCs (Cu6Sn5, Ni3Sn4, Ag3Sn) in the solder matrix.

## Acknowledgment

We appreciate the support of Dr. Young-Boo Lee and Hyang-Ran Moon at the Korea Basic Science Institute for the EPMA analysis, and the support of Sung-Soon Bai of KAIST central research instrument facility for the EBSD analysis.

## References


1. S.K. Kang and A.K. Sarkhel, *J. Electron. Mater.* 23, 701 (1994).

2. S.W. Jeong, J. H. Kim, and H. M. Lee, *J. Electron. Mater.* 33, 1530 (2004).

3. Y.H. Jo, J.W. Lee, S.-K. Seo, H.M. Lee, H. Han and D.C Lee, *J. Electron. Mater.* 37, 110 (2008).

4. S.K. Kang, W.K. Choi, D.-Y. Shih, D.W. Henderson, T. Gosselin, A. Sarkhel, C. Goldsmith, and K.J. Puttlitz, *JOM*, 55 (6), 61(2003).

5. W.K. Choi, S.W. Yoon, H.M. Lee, *Mater. Trans.* 42, 783 (2001).

6. S.-K. Seo, M.G. Cho, W.K. Choi, H.M. Lee. *J. Electron. Mater.* 35, 1975 (2006).

7. D.H. Kim, M.G. Cho, S.-K. Seo, H.M. Lee, *J. Electron. Mater.* 38, 39 (2009).

8. M.G. Cho, S.K. Kang, D.-Y. Shih, H.M. Lee, *J. Electron. Mater.* 36, 1501 (2007).

9. S.K. Kang, M.G. Cho, D-Y. Shih, S.-K. Seo, and H.M. Lee, *Proc. 58$^{th}$ Electronic Components and Technology Conf.* (Piscataway NJ: IEEE, 2008), pp. 478-484.

10. S.-K. Seo, M. G. Cho and H. M. Lee, *J. Electron. Mater.* 36, 1536-1544 (2007).

11. W.P. Mason and H.E. Bommel, *J. Acoust. Soc. Amer.*, 28, 930 (1956).

12. J.A. Rayne and B.S. Chandrasekhar, *Phys. Rev.* 120, 1658 (1960).

13. B.F. Dyson, *J. Appl. Phys.* 37, 2375 (1966).

14. B.F. Dyson, T.R. Anthony, and D. Turnbull, *J. Appl. Phys.* 37, 3408 (1967).

15. D.C. Yeh and H.B. Huntington, *Phy. Rev. Lett.* 53(15), 1469 (1984).

16. F.H. Huang and H.B. Huntington, *Phys. Rev. B* 9(4), 1479 (1974).

17. M. Lu, D.-Y. Shih, P. Lauro, C. Goldsmith, and D.W. Henderson, *Appl. Phys. Lett.* 92, 211909 (2008).

18. M. Lu, P. Lauro, D.-Y. Shih, R. Polastre, C. Goldsmith, D.W. Henderson, H. Zhang, and M.G. Cho, *Proc. 58th Electronic Components and Technology Conf.* (Piscataway NJ: IEEE, 2008), pp. 360-365.

19. D.W. Hendrson, J.J. Woods, T.A. Gosselin, J. Bartelo, D.E. King, T.M. Korhonen, M.A. Korhnen, L.P. Lehman, E.J. Cotts, S.K. Kang, P. Lauro, D.-Y. Shih, C. Goldsmith, and K.J. Puttlitz, *J. Mater. Res.* 19, 1608 (2004).

20. S.K. Kang, P. Lauro, D-Y. Shih, D.W. Henderson, T. Gosselin, J Bartelo, S.R. Cain, C. Goldsmith, K.J. Puttlitz, and T.-K. Hwang, *Proc. 54th Electronic Components and Technology Conf.* (Piscataway NJ: IEEE, 2004), pp. 661-667.

21. L.P. Lehman, S.N. Athavale, T.Z. Fullem, A.C. Giamis, R.K. Kinyanjui, M. Lowenstein, K. Mather, R. Patel, D. Rae, J. Wang, Y. Xing, L. Zavalij, P. Borgesen, and E.J. Cotts, *J. Electron. Mater.* 33, 1429 (2004).

22 A.U. Telang, T.R. Bieler, S. Choi, and K.N. Subramanian, *J. Mater. Res.* **17**, 2294 (2002)

23. S.-K. Seo, S.K. Kang, D.-Y. Shih, and H.M. Lee, *J. Electron. Mater.* **38**, 257 (2009).

24. S.-K. Seo, S.K. Kang, D.-Y. Shih, and H.M. Lee, *Microelectron. Reliab.* (2008), doi:10.1016/j.microrel.2008.11.014

25. B. Sundman, B. Jansson and J.O. Andersson, *CALPHAD*, 9, 153 (1985).

26. J.-H. Shim, C.-S.Oh, B.-J. Lee and D.N. Lee, *Z. Metallkd.* 87, 205 (1996).

27. G. Ghosh, *Met. Mater. Trans. A*, 30A, 1481 (1999).

28. K.-W. Moon, W.J. Boettinger, U.R. Kattner, F.S. Biancaniello, and C.A. Handwerker, *J.Electron. Mater.* 29, 1122 (2000)

29. S.-W. Chen, C.-N. Chiu, and K.-C. Hsieh, *J.Electron. Mater.* 36, 197 (2007).

30. F. Gao, C.P. Wang, X.J. Liu, and K. Ishida, *J.Electron. Mater.* 37, 279 (2008).

31. G.F. Bolling, J.J. Kramer and W.A. Tiller, *Trans. Met. Soc. AIME*, 227, 1453-4 (1963).

32. F. Weinberg, *Trans. Met. Soc. AIME*, 221, 844-850 (1961).

## Tables

Table 1. Anisotropic properties of Sn [11-16].

| | Coefficient of thermal expansion (ppm/°C) [11] | Young's modulus, E (Gpa) [12] | Diffusivity in Sn (at 150°C) ($cm^2$/sec) | | | Sn self-diffusivity (at 150°C) ($cm^2$/sec) [16] |
|---|---|---|---|---|---|---|
| | | | Ag [13] | Cu [14] | Ni [15] | |
| a-axis | 15.45 | 22.9 | $5.60 \times 10^{-11}$ | $1.99 \times 10^{-7}$ | $3.85 \times 10^{-9}$ | $8.70 \times 10^{-13}$ |
| c-axis | 30.50 | 68.9 | $3.13 \times 10^{-9}$ | $8.57 \times 10^{-6}$ | $1.17 \times 10^{-4}$ | $4.71 \times 10^{-13}$ |

Table 2. EPMA quantitative composition analysis of Sn-rich solder/Cu joints and the thermodynamic calculation of Cu solubility in solders.

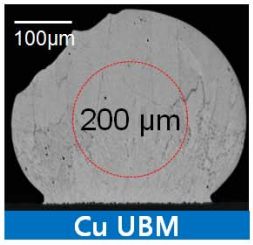


| | EPMA composition analysis (diameter of area: 200μm) (wt %) | | | The thermodynamic calculation of Cu solubility in solders (wt %) |
|---|---|---|---|---|
| | Cu | Ag | Sn | |
| Sn100/Cu | 1.31 | · | balance | 1.23 (in Sn-Cu system) |
| Sn0.5Cu/Cu | 1.26 | · | balance | |
| Sn0.5Ag/Cu | 1.23 | 0.61 | balance | 1.21 (in Sn-Ag-Cu system) |
| Sn1.8Ag/Cu | 1.27 | 1.87 | balance | 1.16 (in Sn-Ag-Cu system) |

Table 3. EPMA quantitative composition analysis of Sn-rich solder/Ni(P) joints and the thermodynamic calculation of Ni solubility in solders.

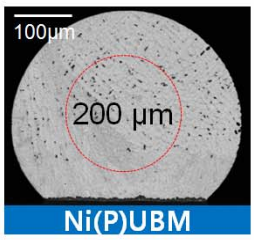


| | EPMA quantitative analysis (diameter of area: 200um) (wt %) | | | | The thermodynamic calculation of Ni solubility in solders (wt %) |
|---|---|---|---|---|---|
| | Ni | Cu | Ag | Sn | |
| Sn100/Ni | 0.13 | | · | balance | 0.20 (in Sn-Ni system) |
| Sn0.5Cu/Ni | 0.07 | 0.51 | · | balance | 0.06 (in Sn-Cu-Ni system) |
| Sn0.5Ag/Ni | 0.18 | | 0.45 | balance | 0.19 (in Sn-Ag-Ni system) |
| Sn1.8Ag/Ni | 0.16 | | 1.81 | balance | 0.18 (in Sn-Ag-Ni system) |

## Figures

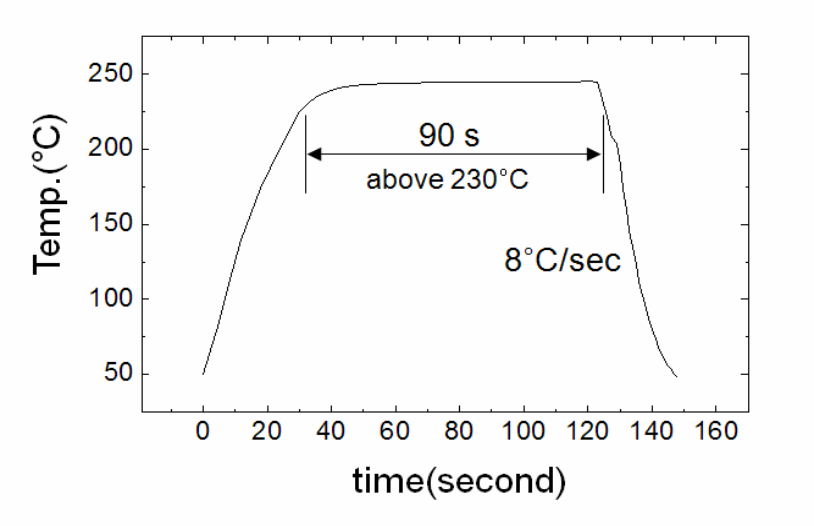


Figure 1. Heat profile during reflow.

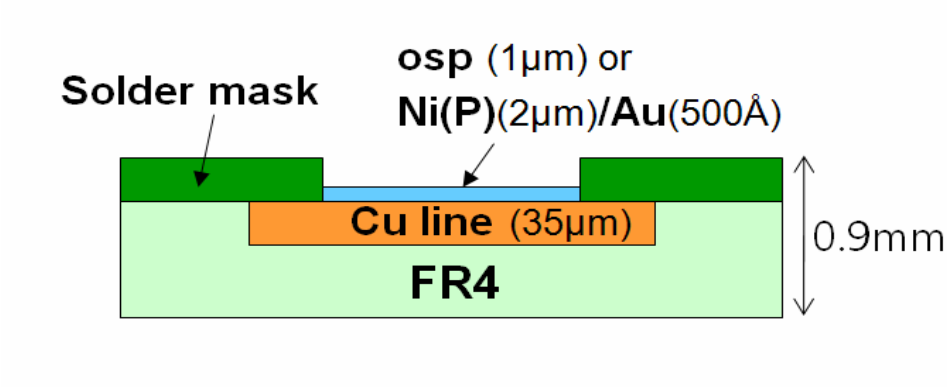


Figure 2. PCB design with two different UBM structure (Cu line/osp finish or Cu line/Ni(P)/Au finish).

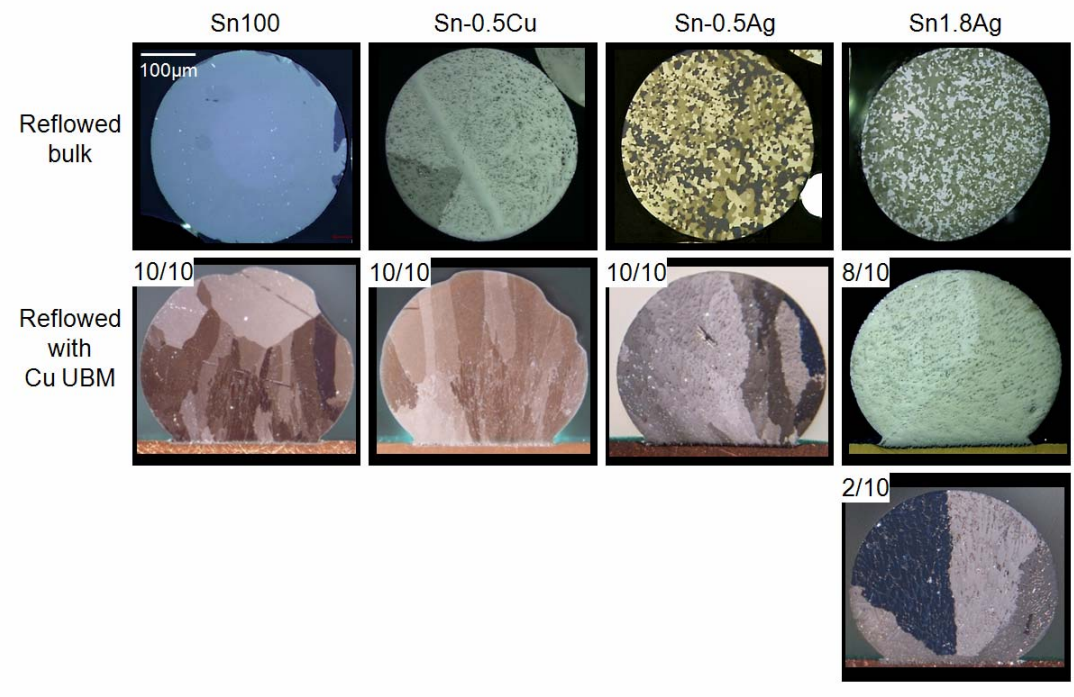


Figure 3. Cross-polarized images of reflowed bulk solders and solder joints reflowed with Cu UBM.

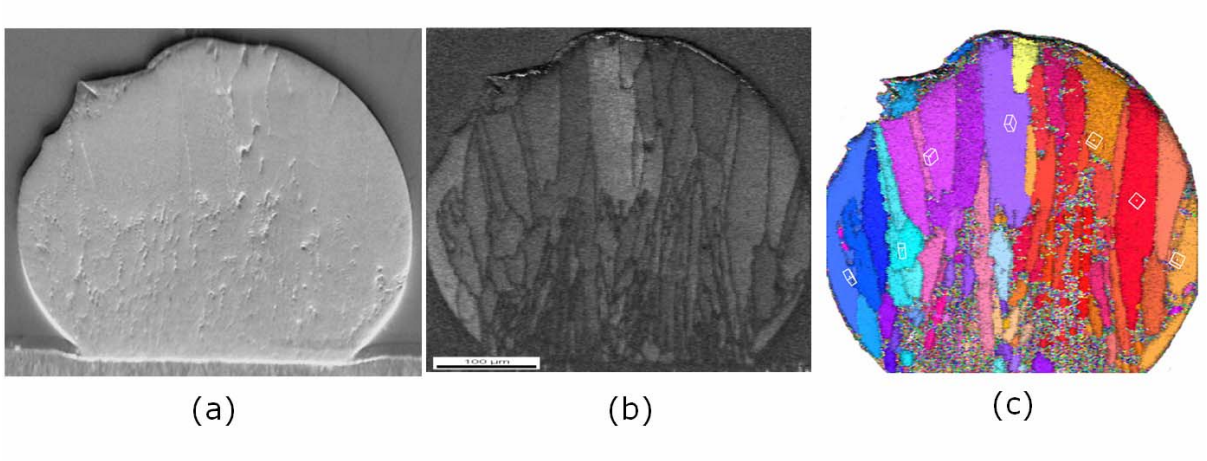


Figure 4. EBSD analysis of Sn-0.5Cu/Cu joint (a) SEM image, (b) image quality map, (c) inverse pole figure map.

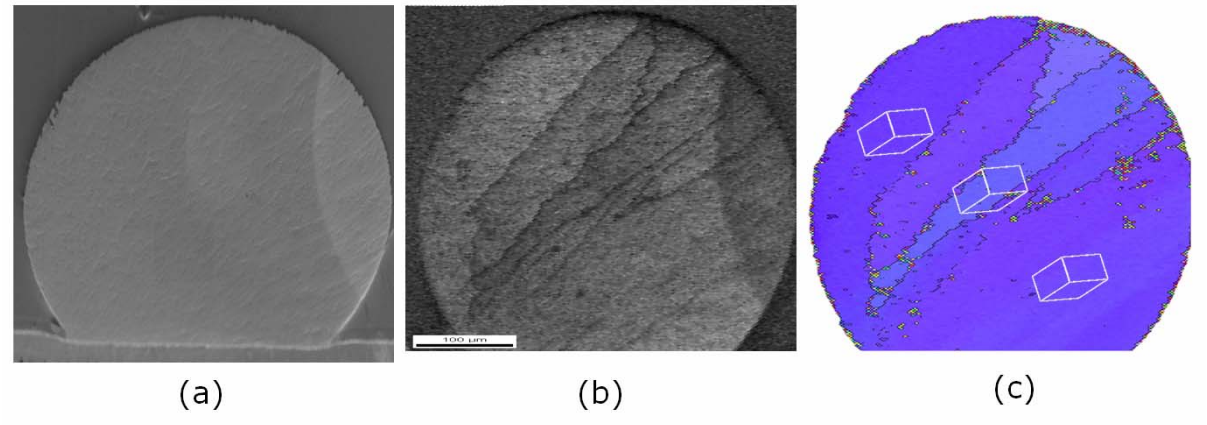


Figure 5. EBSD analysis of Sn-1.8Ag/Cu joint (a) SEM image, (b) image quality map, (c) inverse pole figure map.

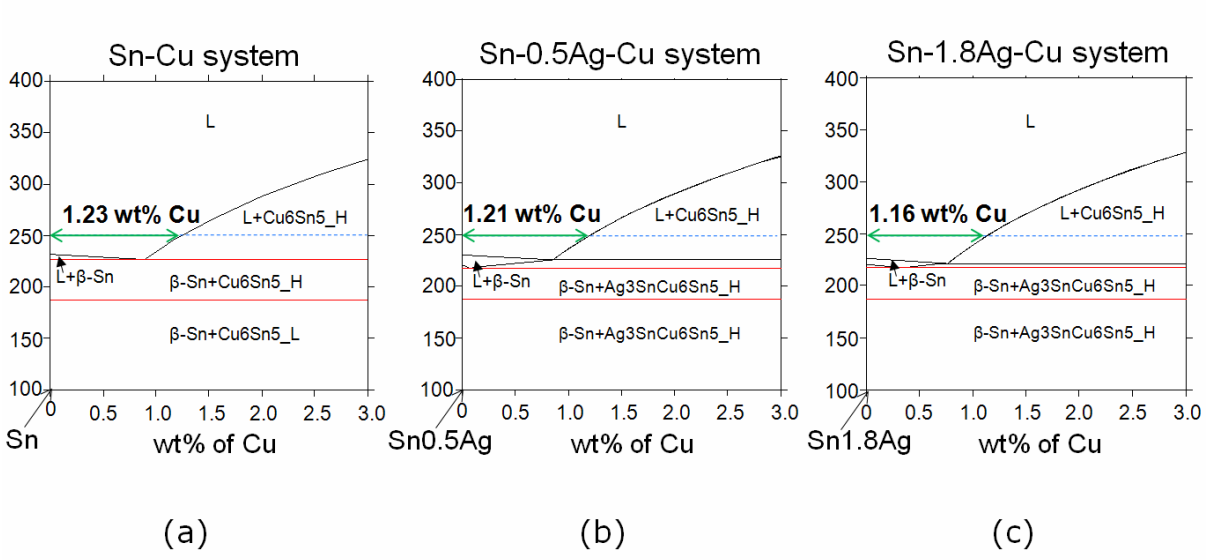


Figure 6. The thermodynamic calculation of Cu solubility of Sn-rich solders at 250°C in (a) Sn-Cu binary phase diagram, (b) Sn-0.5Ag-Cu ternary phase diagram, and (c) Sn-1.8Ag-Cu ternary phase diagram.

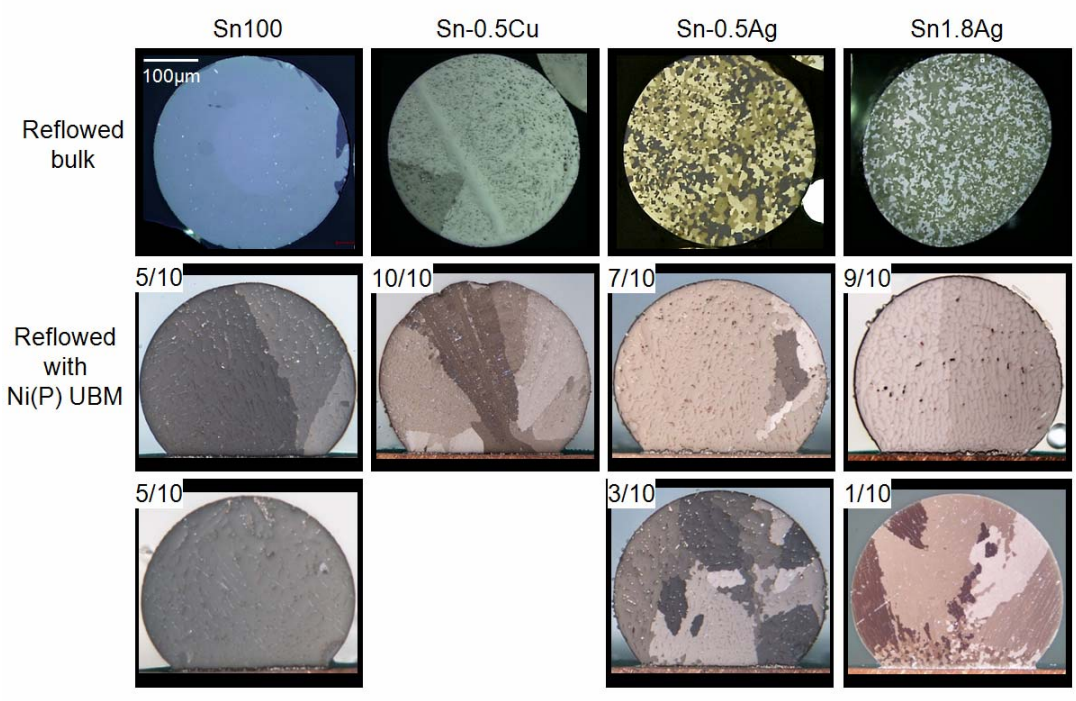


Figure 7. Cross-polarized images of of reflowed bulk solders and solder joints reflowed with Ni(P) UBM.

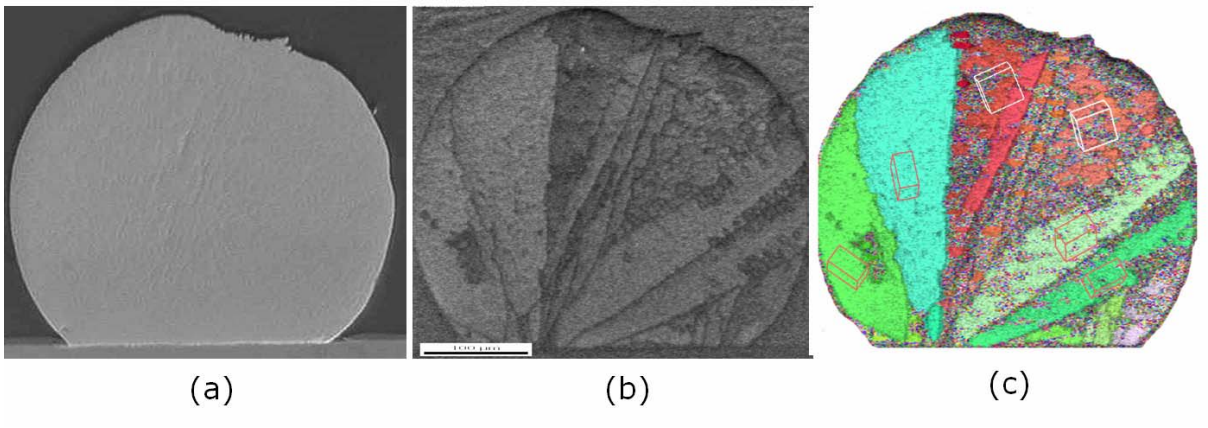


Figure 8. EBSD analysis of Sn-0.5Cu/Ni joint (a) SEM image, (b) image quality map, (c) inverse pole figure map.

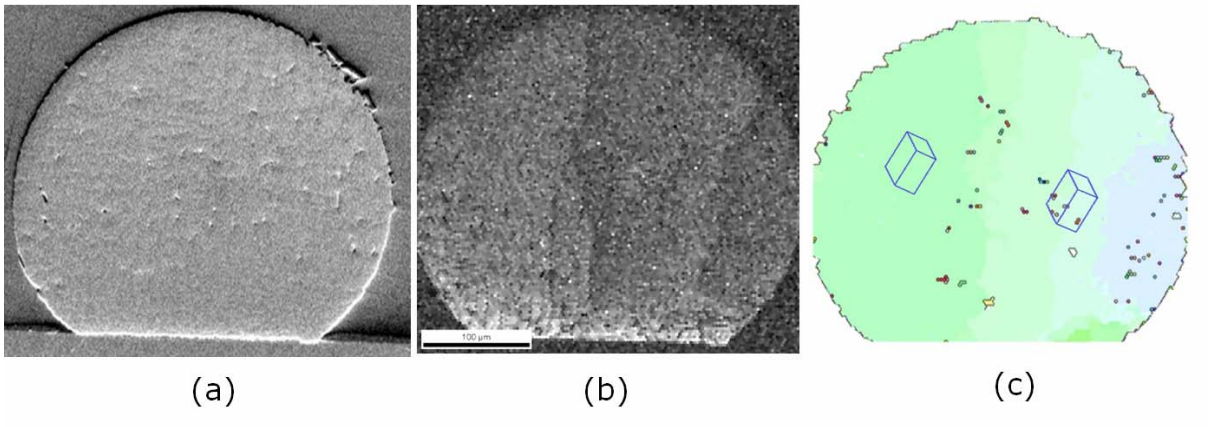


Figure 9. EBSD analysis of Sn-1.8Ag/Ni joint (a) SEM image, (b) image quality map, (c) inverse pole figure map.

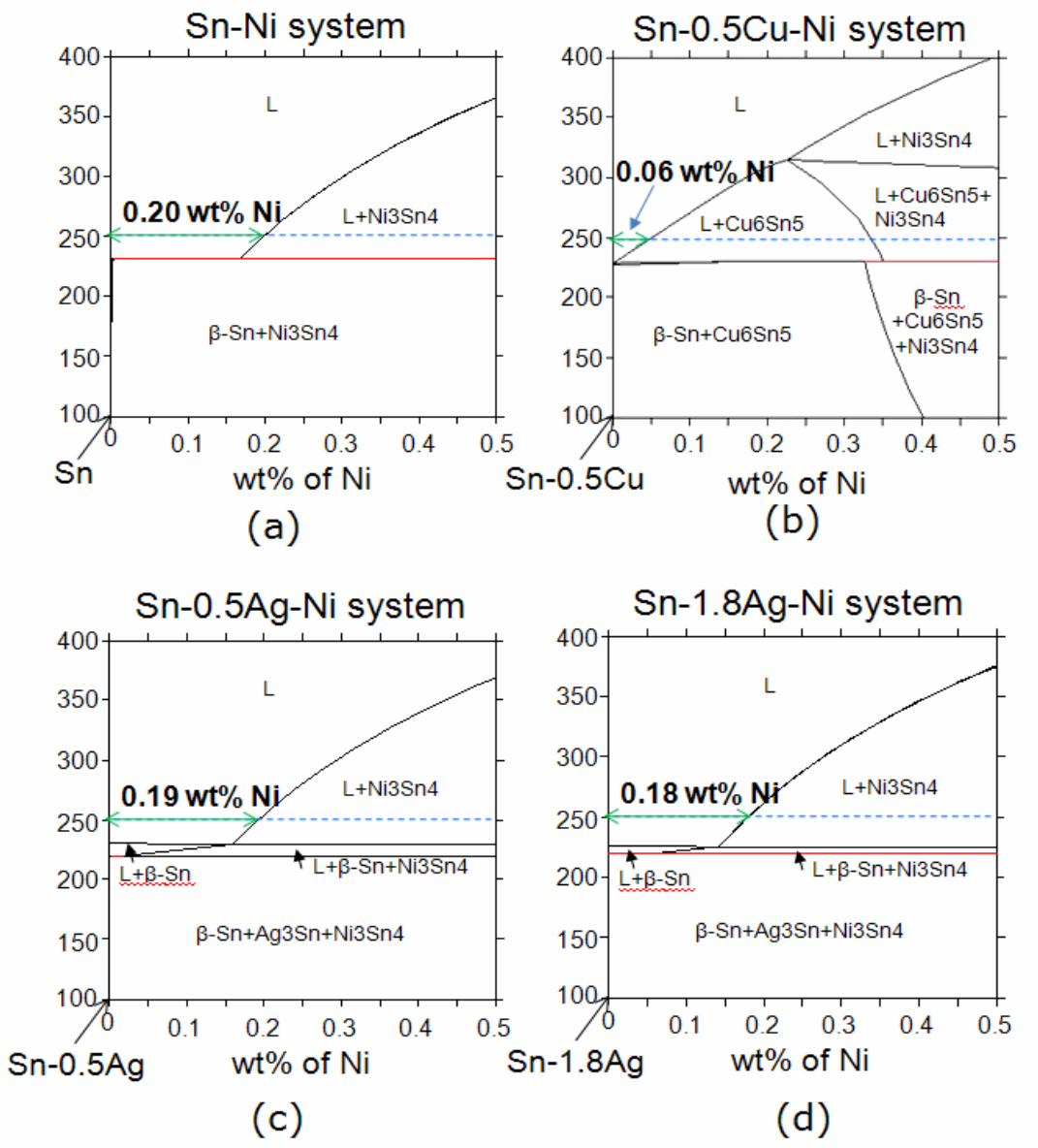


Figure 10. The thermodynamic calculation of Ni solubility of Sn-rich solders at 250°C in (a) Sn-Ni binary phase diagram, (b)Sn-0.5Cu-Ni ternary phase diagram, (c) Sn-0.5Ag-Ni ternary phase diagram, and (d) Sn-1.8Ag-Ni phase diagram.